arXiv:1107.1926v2 [cond-mat.stat-mech] 3 Jan 2012

Nanoparticle Confinement in Anomalous Liquids

Elena G. Strekalova,[1] Jiayuan Luo,[1] H. Eugene Stanley,[1]
Giancarlo Franzese,[2] and Sergey V. Buldyrev[3]

[1]Center for Polymer Studies and Department of Physics,
Boston University, Boston, Massachusetts 02215, USA
[2]Departament de Física Fonamental, Universitat de Barcelona,
Diagonal 645, 08028 Barcelona, Spain
[3]Department of Physics, Yeshiva University,
500 West 185th Street, New York, New York 10033, USA

(Dated: January 4, 2012)

Abstract

We investigate using molecular dynamics the effect of the structure of nanoconfinement for liquids with water-like anomalies and liquid-liquid phase transition (LLPT). We find that if the confinement is in an ordered matrix of nanoparticles (NPs) the anomalies are preserved, although the LLPT shifts to lower temperatures, higher pressures and higher densities with respect to bulk. On the contrary, if the NPs matrix is disordered, we find a drastically different phase diagram: the LLPT occurs only in a reduced interval of densities and the anomalies are washed out. To understand this effect we calculate the changes in the system at the microscopic level. In all the different confinements considered here we observe a dramatic increase of density of liquid near the confining NPs. In the disordered case the confinement induces larger heterogeneity in the local density, responsible for the weakening of the LLPT and the disappearance of anomalies.

PACS numbers: 64.70.Ja,65.20.-w, 66.10.C-

Many experiments in recent years have shown that there is a number of liquids whose properties are highly anomalous [1]. For example, data for liquid metals, metalloids, nonmetals, oxides and alloys, including Ga, Bi Te, S, Be, Mg, Ca, Sr, Ba, SiO_2, P, Se, Ce, Cs, Rb, Co, Ge, $Ge_{15}Te_{85}$ [1], reveal the presence of a temperature of maximum density (TMD) below which the density decreases under isobaric cooling. The most famous example of anomalous liquid is water, whose TMD at 1 atm is at approximately 4^oC. Another anomaly that is attracting considerable attention is the possible existence of a liquid–liquid phase transition (LLPT) for single-component systems. Based on simulations for water [2], it has been proposed that the two coexisting liquids, the high density liquid (HDL) and the low density liquid (LDL), would differ in density and local structure. Liquid polymorphism is observed in experiments on P, [3], $P(OC_6H_5)_3$ [4] and yttrium oxide-aluminum melts [5]. Data consistent with a LLPT arise from experiments for single-component systems, such as water [6], silica [7], C [8], Se [9], Co [10], among others [11]. Here we ask the question how nanoconfinement of an anomalous liquid may change its behavior. The question is relevant for the vast arena of nanotechnological applications and for the lively debate about the properties of confined water in nanoscopic and biological systems [12–15].

To approach the problem we focus on the effects of the structure of a fixed confining matrix of nanoscopic particles (NPs) on the phase diagram of a liquid with anomalous behavior and with a LLPT ending in a liquid-liquid critical point (LLCP). As model liquid we consider (i) a ramp potential [16], and for comparison (ii) a shoulder potential [17].

Potential (i) has a hard-core at distance $r = a$, and a linear ramp for $a < r \leq b$ decreasing from interaction energy $U_R > 0$ to $U_0 < 0$, plus a linear ramp for $b < r \leq c$ increasing from U_R to 0. We adopt $b/a = 1.72$, $c/a = 3$ and $U_R = 3.56U_0$. For this set of parameters the LLCP lies well above the melting line [18]. The interaction with the NPs is modeled by the hard sphere repulsion.

Potential (ii) has a repulsive shoulder and an attractive well with energy minimum U_0, [17] with parameters chosen to fit a potential proposed for water [19]. The interaction with NPs is given by a $1/r^{100}$ power law that crosses the zero of the interaction energy at the unit distance a. Results presented in the following, if not otherwise indicated, are for the potential (i), with consistent results for potential (ii).

Both potentials (i) and (ii) display water-like anomalies and a LLPT [16, 17]. For both we perform simulations at constant number N of particles, constant volume V and constant temperature T, with periodic boundary conditions. For (i) we employ a discrete molecular dynamics algorithm by discretizing the linear ramp potential into steps, with $\Delta U = U_0/8 = 0.125$ [20]. For (ii) we integrate the equations of motion using velocity Verlet integrator and we adopt the Allen thermostat [17].

We confine the liquid particles in a fixed matrix of $N_{\rm NP} = 64$ nanoparticles of diameter $D_{\rm NP} = 3a$. The liquid particles interact with NPs via hard core repulsion at distance $r_0 = (a + D_{\rm NP})/2$. We consider three different structures for the matrix: a perfect cubic lattice (CUBE); a cubic lattice with Gaussian distortions (DIST) with a standard deviation of 1/4 of the separation between centers of NPs, which still preserves an approximately periodic and ordered structure of the confinement (Fig.1a); and a completely random (RND) configuration of NPs obtained by simulating a gas of hard spheres (Fig.1b). The volume fraction of NPs is $x_{\rm NP} = V_{\rm NP}/V = 24.5\%$ in a cubic simulation box with fixed volume $V/a^3 = (20.6)^3$, and $V_{\rm NP}/a^3 = N_{\rm NP} 4\pi(r_0/a)^3/3$ volume of NP. We repeat the analysis for a random configuration of NPs with diameter $5a$, keeping constant $x_{\rm NP}$ and the size of the simulation box. We control $\rho = N/(V - V_{\rm NP})$ of liquid particles by adjusting N. We account for the excluded volume by rescaling the pressure P by $V/(V - V_{\rm NP})$.

For potential (i), the bulk liquid displays a LLCP at $k_B T_C^{\rm bulk}/U_0 = 0.375$, $P_C^{\rm bulk} a^3/U_0 = 0.243$, and $\rho_C^{\rm bulk} a^3 = 0.37$ [16]. Figures 1(c) and 1(d) show simulated isochores for DIST and RND confinement, respectively, with the HDL-LDL spinodal lines calculated from $(\partial P/\partial \rho)_T = 0$ and $(\partial^2 P/\partial \rho^2)_T \neq 0$, and the LLCP obtained from the merging of the spinodal lines where $(\partial P/\partial \rho)_T = (\partial^2 P/\partial \rho^2)_T = 0$. For each confinement we find that the LLCP shifts to lower T, higher ρ, and higher P relative to the bulk liquid (Fig.2a). As the disorder in the confining matrix increases, T shift becomes more pronounced while ρ and P shifts are reduced. We find the same qualitative trend in the LLCP shifts for the liquid with potential (ii), and a progressive approach of the LLCP to the bulk case when the NPs concentration decreases (Fig.2b), consistent with previous results for NP-liquid mixtures [14].

Although the periodic DIST confinement preserves the LDL-HDL coexistence region observed in bulk liquid [16], which is consistent with a strong first-order LLPT, the RND confinement shrinks the coexistence region (Figs. 1c and 1d), hinting at a weakening in the LLPT. This weakening is qualitatively consistent with recent numerical results for supercooled water in random hydrophobic pore-like confinement [15].

The region of density anomaly is bounded by the lines of TMD and temperature of minimum density (TminD) located by the extrema of the isochores. In the bulk system the TminD line for high densities is hindered by the glass transition line and cannot be observed in the equilibrium liquid. Here we observe that the periodic structure of the confinement can dramatically affect density anomaly manifestations. Comparatively to the bulk, confinement decreases TMD and increases TminD, shrinking the T range of the density anomaly. While for the DIST confinement the density anomaly is still well defined, it appears much less pronounced in RND case. For a RND matrix of large confining NPs with diameter $5a$, TMD and TminD are completely absent (not shown).

To understand the origin of the different effects for the different confinements, we first study the density of the liquid in the vicinity of NPs. We find that a layer of liquid adsorbs onto the NPs, as emphasized by the NP-liquid particle radial distribution functions $g_{\mathrm{NP-liq}}(r)$(Fig.3a). We understand the increase of density near the NP surface as a consequence of the maximization of entropy. By sticking to the fixed NPs, the adsorbed liquid particles allow more free space to the the rest of the liquid, maximizing the entropy of the system (depletion effect). This result evokes a similar effect found for water forming a high-density layer of ≈ 5 Å at confining surfaces, regardless of the hydrophobic or hydrophilic interaction with the surface [21–23].

We find that, by increasing randomness in the confinement, the probability of overlap of NP exclusion volumes increases and the depletion effect decreases. As a consequence, the density of liquid near the NPs decreases (Fig.3b). In addition, we analyze the density fluctuations and the associated measurable response function, the isothermal compressibility K_T (Fig.3a), of the liquid in the vicinity of the NPs. We find that the local K_T is extremely small right at the interface, consistent with a tight packing of liquid particles around the NPs. Near the first minimum of $g_{\mathrm{NP-liq}}(r)$ the local K_T is, instead, twice as high as the bulk, consistent with [21]. High vicinal density of liquid rationalizes the density increase of the LLCP (Fig.2), because, when part of the liquid is adsorbed onto the NPs, an average liquid density larger than bulk is necessary to build up the critical fluctuations. The shift is more pronounced for CUBE and DIST confinement, with respect to RND, because the more ordered the confinement the larger the NP surface available for the depletion effect.

To understand the distribution of local density inside the simulation box, we performed Delaunay tessellation for a set of NPs in both RND and DIST confinements, partitioning the total volume into space-filling irregular tetrahedra with four nearest neighbor NPs as vertices (Fig.4a,b insets). We find that the RND confinement, with respect to the DIST case, induces a larger heterogeneity in the distribution of local densities ρ_v in each tetrahedra at any fixed value of the global density ρ (Fig.4a,b). The significant overlap of ρ_v distributions for the HDL and the LDL phases in RND confinement (Fig.4a) suggests the presence of disordered mesoporous microdomains of various densities (Fig.1d insets) that contribute to the weakening of the LLPT. This is not observed in DIST case (Fig.4b), where the distributions of ρ_v are closely centered around the average global ρ with no overlap between HDL and LDL phases, preserving a strong LLPT.

The fact that for RND confinement the local density is more heterogeneous and the liquid-liquid coexistence occurs at the local scale within Delaunay tetrahedra, allows us to rationalize the T-decrease of the LLCP with respect to the more ordered confinements and the bulk. Local heterogeneity inhibits the global LLPT, driving the LLCP temperature to a lower value. Due to the positive slope of the LLPT, the decrease of LLCP temperature implies a decrease of the LLCP pressure (Fig. 2). The presence of density heterogeneity, along with the reduced depletion effect in the RND confinement matrix, gives us the key to understand the differences between ordered and disordered confinement.

In conclusion, we predict that anomalous liquids, with a LLPT, preserve their bulk phase diagram and density anomalies when are confined in a matrix of periodically ordered NPs. Moreover, in the case of small distortion of the ordered confinement, the homogeneous crystal nucleation is inhibited at temperatures lower than in bulk, allowing the direct observation of the TminD locus. A strong depletion effect induces a large increase of density in the vicinity of the NPs. The effect is smaller when the confinement has a random structure. Randomness induces the occurrence of disordered density domains weakening the LLPT, narrowing the LLPT coexistence region, and washing out the density anomalies.

It is interesting to mention that these results could qualitatively explain recent experiments for confined water, the prototypical anomalous liquid. While the TminD locus has been observed in supercooled water under hydrophilic confinement by MCM-41 silica nanoporous matrix [24], its absence has been reported in hydrophobic mesoporous material CMK [25]. MCM-41 forms a very regular matrix [24], while CMK consists of grains, each with a disordered, 3D interconnected bicontinuous, pore structure [25]. Therefore, as shown in our model for a generic anomalous liquid, the disparity of results for different kinds of confinements may arise from the different amount of disorder in the confining structures.

We thank D. Corradini, P. Gallo and K. Stokely for discussions. EGS, JL, and HES acknowledge the support of NSF grants CHE0908218 and CHE0911389, SVB the partial support of the Dr. Bernard W. Gamson Computational Science Center at Yeshiva College, and GF of Spanish MICINN grant FIS2009-10210 (co-financed FEDER) and the European Union FP7 grant NMP4-SL-2011-266737.

[1] P. Vilaseca, G. Franzese, J. Non-Crys. Sol. **357** 419 (2011) and references therein.

[2] P. H. Poole, et al. Nature (London) **360**, 324 (1992).

[3] Y. Katayama, et al. Nature (London) **403**, 170 (2000); Science **306**, 848 (2004); G. Monaco, et al. Phys. Rev. Lett. **90**, 255701 (2003).

[4] R. Kurita and H. Tanaka, Science **306**, 845 (2004); J. Phys.: Condens. Matter **17**, L293 (2005); H. Tanaka, et al. Phys. Rev. Lett. **92**, 025701 (2004).

[5] G. N. Greaves, et al. Science **322**, 566 (2008).

[6] O. Mishima, J. Chem. Phys. **133**, 144503 (2011).

[7] C. A. Angell, et al. J. Non-Cryst. Solids **207**, 463 (1996); D. J. Lacks, Phys. Rev. Lett. **84**, 4629 (2000).

[8] M. van Thiel and F. H. Ree, Phys. Rev. B **48**, 3591 (1993).

[9] V. V. Brazhkin, et al. Rev. High Pressure Sci. Technol. **7**, 1129 (1998).

[10] M. G. Vasin and V. I. Ladýanov, Phys. Rev. E **68**, 051202 (2003).

[11] S. Aasland and P. F. McMillan, Nature (London) **369**, 633 (1994); M. C. Wilding and P. F. McMillan, J. Non-Cryst. Solids **293**, 357 (2001); M. C. Wilding, et al. *ibid* **297**, 143 (2002).

[12] M. Majumder, et al. Nature **438**, 44 (2005); S. Joseph and N. R. Aluru, Phys. Rev. Lett. **101**, 064502 (2008).

[13] F. Mallamace, et al. J. Phys.: Condens. Matter **18**, S2285 (2006); Proc. Natl. Acad. Sci. **104**, 424 (2007); S.-H. Chen and C. K. Loong, Nucl. Eng. and Tech. **38**, 201 (2006); D. Liu, et al. J. Phys. Chem B **112**, 4309 (2008).

[14] D. Corradini, Phys. Rev. E. **81** 061504 (2010).

[15] E. G. Strekalova, et al. Phys. Rev. Lett. **106**, 145701 (2011).

[16] E. A. Jagla, Phys. Rev. E **63**, 061501 (2001); L. Xu, et al. Proc. Natl. Acad. Sci. **102**, 16558 (2005); Phys. Rev. E **74**, 031108 (2006).

[17] G. Franzese, J. Mol. Liq. **136**, 267 (2007); A. B. de Oliveira, et al. J. Chem. Phys. **128**, 064901 (2008); P. Vilaseca, and G. Franzese, *ibid.* **133**, 084507 (2010).

[18] L. Xu, et al. J. Chem. Phys. **130**, 054505 (2009).

[19] T. Head-Gordon and F. H. Stillinger, J. Chem. Phys. **98**, 3313 (1993).

[20] S. V. Buldyrev, Lect. Notes Phys. **752**, 97 (2008).

[21] R. Godawat, S. N. Jamadagni, and S. Garde, Proc. Natl. Acad. Sci. **106**, 15119 (2009).

[22] G. Cicero, et al. J. Am. Chem. Soc. **130**, 1871 (2008).

[23] T. Werder, et al. J. Phys. Chem. B **107**, 1345 (2003); J. Marti, et al. J. Chem. Phys. **124**, 094703 (2006); M. C. Gordillo and J. Marti, Phys. Rev. B **78**, 075432 (2008).

[24] F. Mallamace, et al. Proc. Natl. Acad. Sci. **104**, 18387 (2007).

[25] Y. Zhang, et al. J. Phys. Chem. B **113**, 5007 (2009).

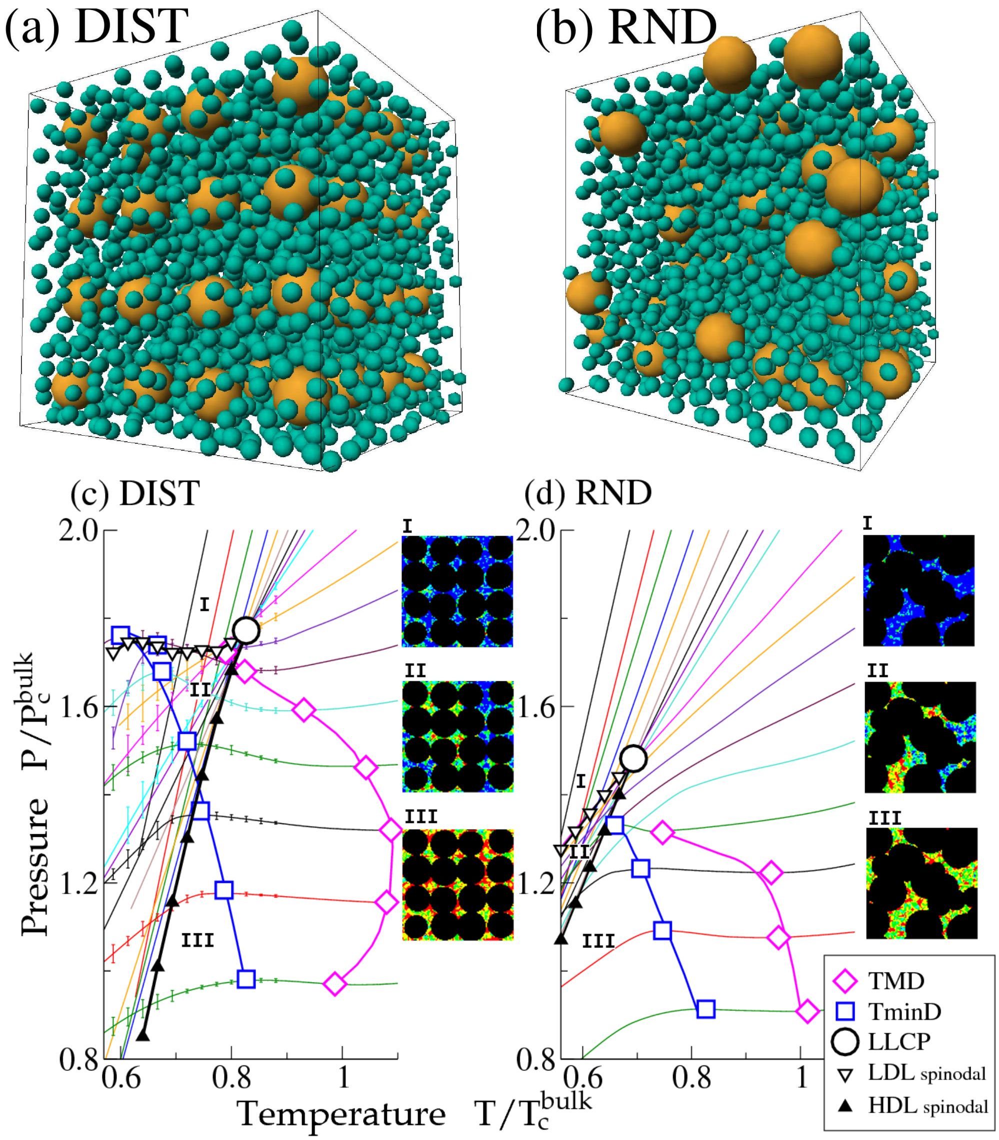

FIG. 1: Effect of confinement. Snapshots of the anomalous liquid (green) confined in a fixed matrix of NPs (yellow) in a DIST (a) and RND (b) configuration. Polynomial fits of simulated isochores of densities $0.89 \leq \rho/\rho_C^{\rm bulk} \leq 1.59$ (bottom to top at $T/T_C = 1$) for DIST (c) and RND (d). Randomness reduces the temperature and pressure of the LLCP (circles), the separation between the HDL (lower filled triangles) and LDL spinodals (upper open triangles) and the separation between the TMD (diamonds) and the temperature of minima of densities (TminD, squares). Samples of error bars on P are given in panel (c). Lines connecting symbols are guides for the eyes. Insets: cuts through the simulation box at density above (I), between (II) and below (III) the coexistence densities. The black circles (with a maximal radius of $3.5a$) mark regions where liquid particles stick to the NPs, as discussed in the text. Outside these regions the liquid density is represented by a color code going from blue (high liquid density) to red (low liquid density).

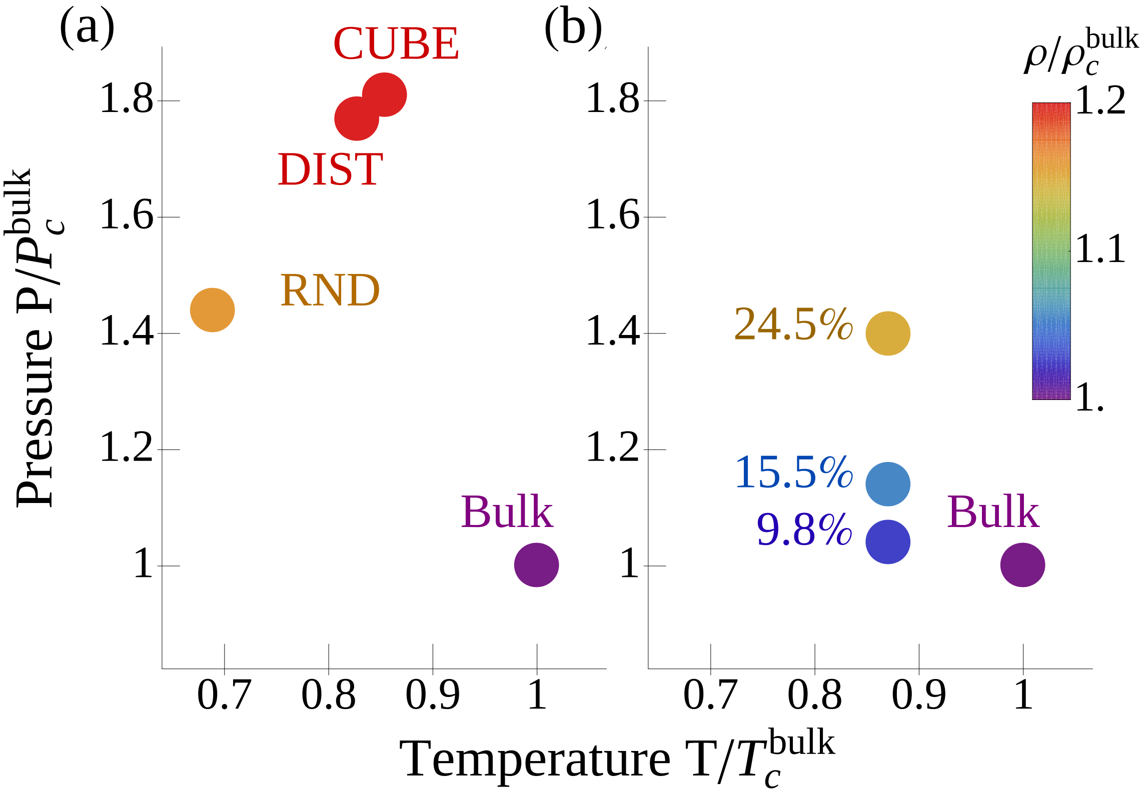

FIG. 2: The confinement affects the parameters of the LLCP. Color-coded circles represent the LLCP parameters in the $P-T-\rho$ phase space (a) for the liquid confined in the fixed matrix of NPs with CUBE, DIST and RND configuration. Increasing disorder in the confinement, from CUBE to DIST to RND, shifts the LLCP down in ρ, T, and P. (b) Upon decreasing concentration $x_{\rm NP}$ (label near the symbols) for the CUBE confinement of the liquid with potential (ii), the LLCP approaches the bulk case. We find the same behavior for potential (i).

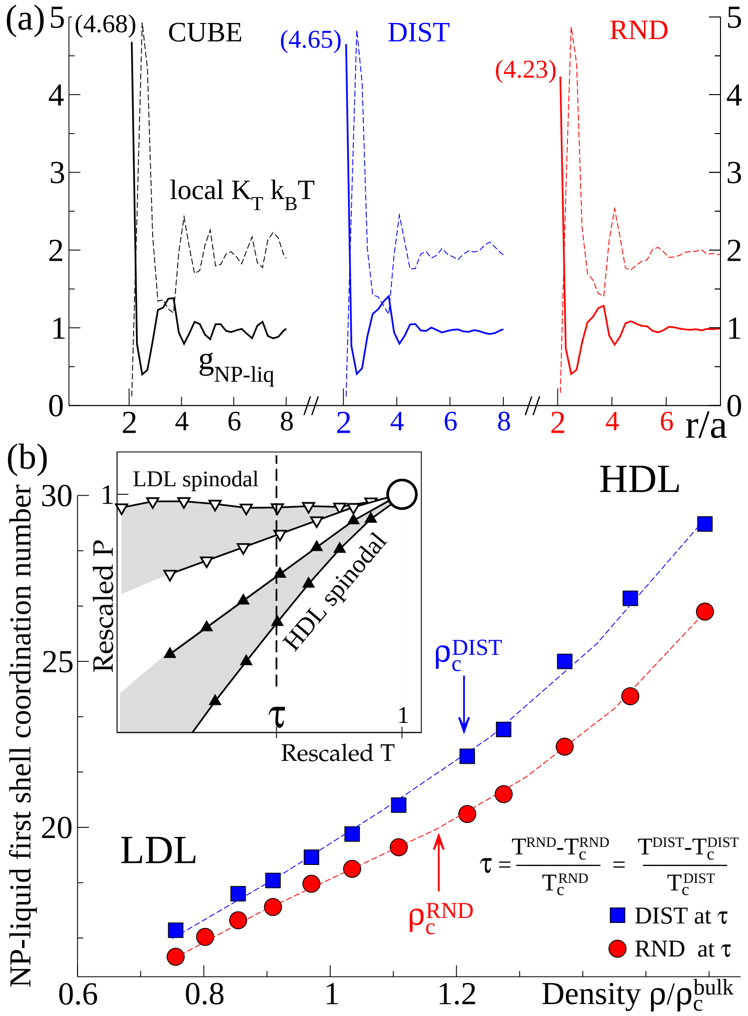

FIG. 3: (a) The liquid adsorbs onto the NPs. The NP-liquid particle radial distribution functions $g_{\text{NP-liq}}(r)$ at $T/T_C^{\text{bulk}} = 1.12$ for CUBE (leftmost), DIST (center) and RND (rightmost) confinements for density $\rho/\rho_c^{\text{bulk}} = 1.59$ (thick lines) display large maxima (in parenthesis) at the closest NP-liquid particle distance $r = r_0 \equiv 2a$. Normalized local compressibility $K_T k_B T$ (broken lines) computed from the fluctuations of the number of particles in volume $5.5a^3$ shows large peaks near the minimum of $g_{\text{NP-liq}}(r)$. The results for different confinements are shifted horizontally for clarity. (b) Number of liquid particles adsorbed onto a NP, at a distance $r_0 \leq r \leq 2.5a$, where the first minimum of $g_{\text{NP-liq}}(r)$ occurs, for DIST (blue squares) and RND (red circles) for a range of densities at fixed rescaled temperature $\tau = (T^{\text{RND}} - T_c^{\text{RND}})/T_c^{\text{RND}} = (T^{\text{DIST}} - T_c^{\text{DIST}})/T_c^{\text{DIST}} = -0.13$. Arrows mark the location of the critical density ρ_c^{RND} (red) for RND and ρ_c^{DIST} (blue) for DIST. Lines are guides for the eyes. (Inset) The rescaled LDL-HDL coexistence region, with the chosen value for τ, for DIST (gray) and RND (white) confinements, ending in the LLCP (circles).

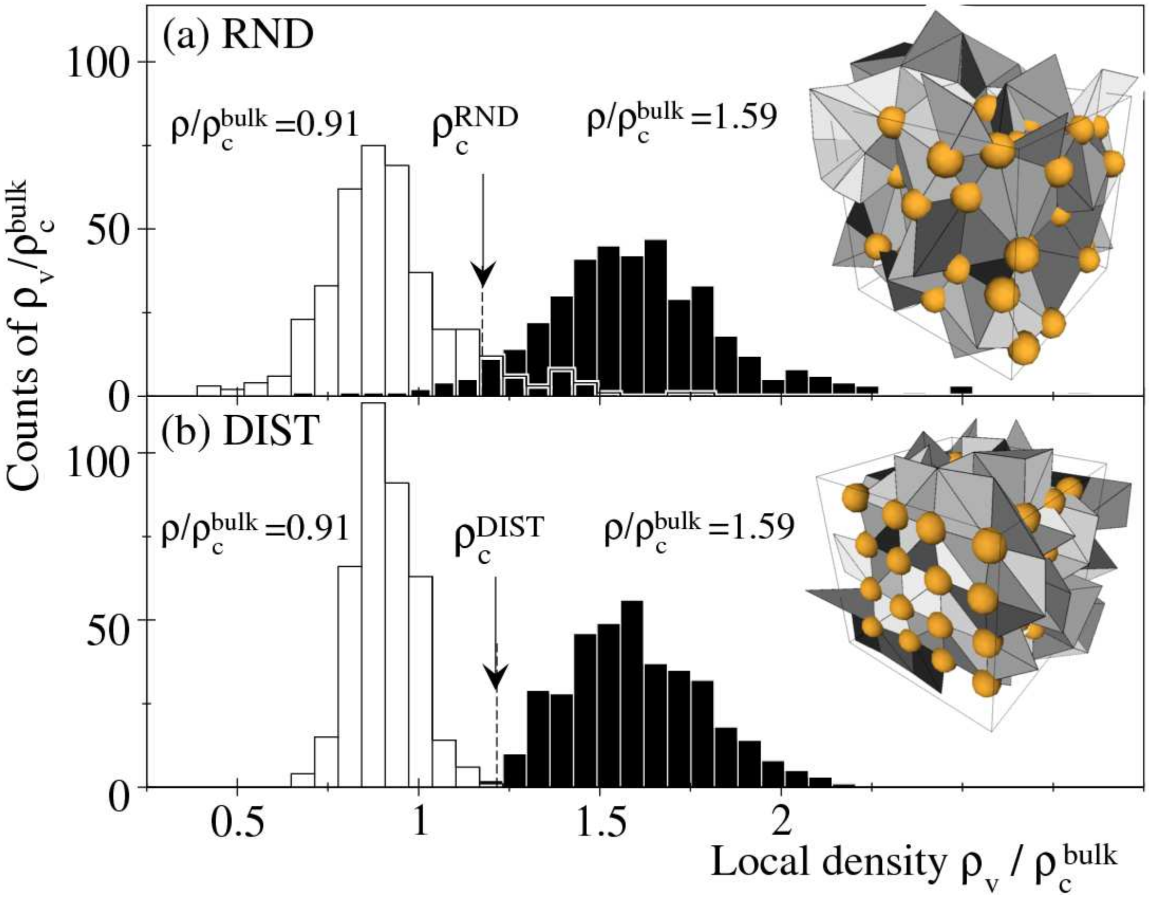

FIG. 4: RND confinement induces heterogeneity in local densities. (a) The distribution of local density $\rho_v/\rho_c^{\mathrm{bulk}}$ of the liquid included in Delaunay tetrahedra of the RND confinement for the LDL global density $\rho/\rho_c^{\mathrm{bulk}} = 0.91$ (white histogram) partially overlaps with that for the HDL $\rho/\rho_c^{\mathrm{bulk}} = 1.59$ (black histogram). (b) The overlap is not present for the DIST case. In both panels an arrow marks the critical density, ρ_c^{RND} for RND and ρ_c^{DIST} for DIST. Insets: Delaunay tetrahedra for RND (top) and DIST (bottom) case, colored according to the value of ρ_v, from high (dark gray) to low (light gray).